Journal of Photochemistry & Photobiology, A: Chemistry 415 (2021) 113314

Contents lists available at ScienceDirect

Journal of Photochemistry & Photobiology, A: Chemistry

journal homepage: www.elsevier.com/locate/jphotochem

Effect of the complex-formation ability of thiosemicarbazones containing (aza)benzene or 3-nitro-1,8-naphthalimide unit towards Cu(II) and Fe(III) ions on their anticancer activity

Roksana Rzycka-Korzec [a,c], Katarzyna Malarz [b,c], Robert Gawecki [b,c], Anna Mrozek-Wilczkiewicz [b,c], Jan Grzegorz Małecki [a], Ewa Schab-Balcerzak [a,d], Mateusz Korzec [a,*], Jaroslaw Polanski [a,c,*]

[a] Institute of Chemistry, University of Silesia in Katowice, Szkolna 9, 40-006 Katowice, Poland
[b] A. Chełkowski Institute of Physics, Universityof Silesia in Katowice, 75 Pułku Piechoty 1, 41-500 Chorzów, Poland
[c] Silesian Centre for Education and Interdisciplinary Research, University of Silesia in Katowice, 75 Pułku Piechoty 1A, 41-500 Chorzów, Poland
[d] Centre of Polymer and Carbon Materials, Polish Academy of Sciences, 34 M. Curie-Sklodowska Street, 41-819 Zabrze, Poland

ARTICLE INFO

Keywords:
Antitumor activity
Thiosemicarbazones
Metal complexing ability
Structure-anticancer activity relationship

ABSTRACT

We recently described a novel class of thiosemicarbazones (TSCs) with a high anticancer activity. Now, we expanded this compound library with a new class of TSCs with a 3-nitro-1,8-naphthalene unit. Thus, a series of novel TSC conjugates was obtained to determine the effect of its chemical structure on spectroscopic properties, metal complexing and biological activity. They were prepared in a microwave reactor, provided compounds with both a high yield and purity. Nuclear magnetic resonance (^{1}H and ^{13}C NMR, COSY, HMQC) and infrared spectroscopy were used to characterize them structurally. Additionally, DFT calculations were performed in order to obtain the optimized ground-state geometry. Physicochemical spectroscopic studies were conducted in different solvents and conditions to assess the effect of the substituent on the optical properties and metal complexing ability. The anticancer activity was tested on three cancer cell lines and then correlated with the spectroscopic results. Here, we show based on *in vitro* chelating studies, that anticancer activity is closely correlated with the Fe^{3+} and Cu^{2+} chelating ability of these compounds.

1. Introduction

Because iron and copper are important for the proper functioning of cells, new chelators that target these microelements are of substantial interest for contemporary medicinal chemistry [1]. Thiosemicarbazones (TSCs) are a class of compounds that have a broad spectrum of biological activity [2–8]. In particular, their antitumor activity is often associated with metal chelating ability, which controls the bioavailability of these metals [9,10]. Moreover, ligand-metal complexes are potential sources of free radicals. TSC complexation can also affect important cellular processes such as cell cycle inhibition and the deactivation of the ribonucleotide reductase (RR) enzyme [11,12]. In particular, this refers to a function of cancer cells [13]. Different oxidation states determine the behavior of metals, which are reactive in redox reactions. Metal coordination by the TSC ligand does not saturate the coordination sphere and therefore oxidation/reduction is still possible [9], while a specific coordination manner enables a switch of an electron [2]. TSC ligands, which leave gaps in the coordination sphere, generate reactive oxygen species (ROS) responsible for the anticancer mechanism of action [14]. An increase of the complexing properties of TSCs could potentially enhance their antitumor activity [15]. In this regard, we carefully tested the complexing behavior of a series of TSC compounds that have a high anticancer activity [12,16–19]. Moreover, the TSC structures were modified by introducing 3-nitro-1,8-naphthaliimide into the TSC scaffold in order to analyze the effect of this moiety on the metal complexing properties. The naphthalimide scaffold can often bind to DNA *via* intercalation [19–23], which is often of substantial importance for the anticancer activity of a variety of drugs. In particular, cytotoxic properties have been demonstrated for 3-nitro-1,8-naphthalimides, which contain a six-membered saturated heterocyclic such as piperazine, morpholine or piperidine [24].

The antitumor activity of the new TSCs with the piperazine,

* Corresponding authors at: Institute of Chemistry, University of Silesia in Katowice, Szkolna 9, 40-006 Katowice, Poland.
E-mail addresses: mateusz.korzec@us.edu.pl (M. Korzec), jaroslaw.polanski@us.edu.pl (J. Polanski).

https://doi.org/10.1016/j.jphotochem.2021.113314
Received 16 February 2021; Received in revised form 13 April 2021; Accepted 19 April 2021
Available online 24 April 2021

morpholine or piperidine fragments was described in our previous publications [12,16–19]. Herein, we expanded this compound library with a new class of TSCs with a 3-nitro-1,8-naphthalene unit (NIT), which was obtained by condensing thiosemicarbazides with 3-nitro-1, 8-naphthalic acid anhydride. In the literature, there is very little information on similar compounds [25,26] that were synthesized in a reaction of 2-amino-benzo[de]isoquinolin-1,3-dione with the corresponding isothiocyanides [25]. We show that the anticancer activity of the TSCs are closely related to their chelating ability. Accordingly, unlike TSCs, which appeared to be a strong complexing agent against Fe^{3+} and Cu^{2+}, the complexing and anticancer activity of the NITs were negligible.

2. Experimental section

2.1. Materials and methods

The ^{1}H, ^{13}C NMR and 2d correlation spectra (HMQC, COSY) were recorded on either a Bruker AC400 or Ascend™ 500 spectrometer. The FT-IR measurements were taken using a Nicolet iS5 FT-IR with a spectral range of 400−4000 cm^{-1}. The mass spectra of the TSCs were recorded using a Varian 500-MS IT mass spectrometer (LR-MS (ESI)). The UV–vis absorption spectra were measured using an Evolution™ 200 UV–vis spectrophotometer for a compound concentration of 10 μM and a 1 cm quartz cell. The melting point was determined using OptiMelt. All of the chemicals and starting materials were commercially available and were used without any further purification. The NMR solvents were purchased from ACROS Organics. The metal salts that were used in the UV–vis surveys were prepared from the corresponding chloride salts and were analytical grade. The solvents for the spectroscopy such as chloroform ($CHCl_3$ – Chempur), methanol (MeOH – Acros Organic), acetonitrile (ACN – Acros Organic) and dimethyl sulfoxide (DMSO – Chempur) were used to investigate the absorption properties.

2.2. Synthesizing the thiosemicarbazones

The general procedure for synthesis of 3-nitro-1,8-naphthalimide (***NITs 1-9***) derivatives and the spectral characteristics (^{1}H, ^{13}C NMR and FT-IR) for the compounds that were obtained is described below.

General synthesis of the NIT

A 3-nitro-1,8-naphthalic anhydride (0.25 mmol) with the appropriate thiosemicarbazide (0.25 mmol, *Tc: 1-9*) was introduced into a tube. Then, 15 mL of ethanol was added, and the tube was sealed with a septum. The reaction was conducted in a microwave reactor for 20 min at 80 °C, 40 W. Next, the mixture was cooled, filtered and washed with ethanol. Then, the product was crystallized from ethyl acetate.

NIT-1:

Product in the form of a yellow powder, yield: 59 %; mp: 275−276 °C; **^{1}H NMR** *(500 MHz, d_6-DMSO, ppm)* δ 10.60 (s, 1 H), 9.56 (d, J = 2.0 Hz, 1 H), 9.02 (d, J = 2.1 Hz, 1 H), 8.87 (d, J = 8.2 Hz, 1 H), 8.75 (d, J = 6.8 Hz, 1 H), 8.12 (t, J = 7.8 Hz, 1 H), 7.62 (d, J = 8.8 Hz, 2 H), 7.03 (d, J = 8.9 Hz, 2 H), 4.15 (m, 4 H), 3.59 (m, 4 H). **^{13}C NMR** *(126 MHz, d_6-DMSO, ppm)* δ 183.19, 161.67, 161.29, 152.84, 146.45, 137.63, 135.18, 133.83, 131.70, 130.99, 129.93, 129.77, 124.29, 124.15, 122.81, 120.54, 113.96, 98.61, 48.05, 45.62; **FT-IR** (KBr, ν, cm-1): 3447 (N—H…O); 3285 (N—H); 3110−2940 (C—H aromatic); 2940−2750 (C—H, aliphatic); 1725 and 1690 (C═O imide); 1606 (N═O); 1540 (N—H); 1520 (C═C aromatic).

NIT-2:

Product in the form of a yellow powder, yield: 75 %; mp: 245−246 °C; **^{1}H NMR** *(500 MHz, d_6-DMSO, ppm)* δ 10.61 (s, 1 H), 9.57 (d, J = 2.3 Hz, 1 H), 9.02 (d, J = 2.3 Hz, 1 H), 8.88 (dd, 1 H), 877–8.75 (m, 1 H), 8.12 (dd, 1 H); 7.29–7.26 (m, 2 H), 7.04–7.00 (m, 2 H), 4.15–4.11 (m, 4 H), 3.32 (s, 4 H). **^{13}C NMR** *(126 MHz, d_6-DMSO, ppm)* δ 183.25, 161.96, 161.30, 149.65, 146.47, 137.63, 135.18, 131.71, 130.99, 129.93, 129.78, 129.18, 124.29, 124.17, 123.12, 122.83, 117.32, 48.57, 47.84. **FT-IR** (KBr, ν, cm-1): 3445 (N—H…O); 3357 (N—H); 3110−2940 (C—H, aromatic); 2940−2750 (C—H, aliphatic); 1731 and 1696 (C═O, imide); 1598 (N═O); 1539 (N—H); 1496 (C═C, aromatic).

NIT-3:

Product in the form of a yellow powder, yield: 73 %; mp: 220−221 °C; **^{1}H NMR** *(500 MHz, d_6-DMSO)* δ 10.45 (s, 1 H), 9.58 (d, J = 2.3 Hz, 1 H), 9.04 (d, J = 2.3 Hz, 1 H), 8.91–8.86 (m, 1 H), 8.77 (dd, 1 H), 8.15–8.11 (m, 1 H), 7.38–7.32 (m, 2 H), 7.30 (m, 2 H), 7.24 (m, 1 H), 4.89 (d, J = 11.9 Hz, 2 H), 3.30 (m, 2 H), 2.96 (m, 1 H), 1.93 (m, 2 H), 1.77–1.69 (m, 2 H). **^{13}C NMR** *(126 MHz, d_6-DMSO)* δ 182.83, 161.77, 161.36,146.49, 145.71, 137.91, 135.17, 131.72, 131.06, 129.94, 129.83, 129.01, 127.17, 126.81. 124.30, 124.23, 122.91, 49.90, 41.87, 33.11; **FT-IR** (KBr, ν, cm-1): 3439 (N—H…O); 3335 (N—H); 3110−2940 (C—H, aromatic); 2940−2750 (C—H, aliphatic); 1729 and 1697 (C═O, imide); 1595 (N═O); 1543 (N—H); 1505 (C═C aromatic).

NIT-4:

Product in the form of a yellow powder, yield: 43 %; mp: 266−258 °C; **^{1}H NMR** *(500 MHz, d_6-DMSO, ppm)* δ 10.61 (s, 1 H), 9.58 (d, J = 2.3 Hz, 1 H), 9.03 (d, J = 2.3 Hz, 1 H), 8.88 (dd, 1 H), 8.76 (dd, 1 H), 8.62 (dd, 1 H), 8.26 (m, 1 H), 8.16–8.11 (m, 1 H), 4.17–4.13 (m, 4 H), 3.70–3.67 (m, 4 H). **^{13}C NMR** *(126 MHz, d_6-DMSO, ppm)* δ 183.60, 161.67, 161.29, 159.59, 146.48, 143.78, 137.64, 137.21, 135.18, 131.72, 131.00, 129.94, 127.19, 125.16, 124.30, 124.18, 122.89, 122.84, 120.18, 119.29, 119.06, 48.53, 47.95. **FT-IR** (KBr, ν, cm-1): 3431 (N—H…O); 3193 (N—H); 3110−2940 (C—H aromatic); 2940−2750 (C—H, aliphatic); 1728 and 1699 (C═O imide); 1611 (N═O); 1599 (N—H); 1539 (C═C, aromatic).

NIT-5:

Product in the form of a yellow powder, yield: 56 %; mp: 271−272 °C; **^{1}H NMR** *(500 MHz, d_6-DMSO, ppm)* δ 10.58 (s, 1 H), 9.57 (d, J = 2.3 Hz, 1 H), 9.03 (d, J = 2.3 Hz, 1 H), 8.88 (d, J = 8.3 Hz, 1 H), 8.75 (d, J = 7.3 Hz, 1 H), 8.43 (d, J = 4.8 Hz, 2 H), 8.12 (m, 1 H), 6.71 (t, J = 4.8 Hz, 1 H), 4.12–4.09 (m, 4 H), 3.90 (m, 4 H). **^{13}C NMR** *(126 MHz, d_6-DMSO, ppm)* δ 183.35, 161.68, 161.46, 161.29, 158.49, 146.47, 137.61, 135.17, 131.71, 130.98, 129.93, 129.78, 124.29, 124.18, 122.84, 111.06, 48.51, 43.09; **FT-IR** (KBr, ν, cm-1): 3423 (N—H…O); 3222 (N—H); 3110−2940 (C—H, aromatic); 2940−2750 (C—H, aliphatic); 1725 and 1685 (C═O, imide); 1591 (N═O); 1555 (N—H); 1539 (C═C, aromatic).

NIT-6:

Product in the form of a yellow powder, yield: 54 %; mp: 249−250 °C; **^{1}H NMR** *(500 MHz, d_6-DMSO, ppm)* δ 10.58 (s, 1 H), 9.57 (d, J = 2.3 Hz, 1 H), 9.02 (d, J = 2.3 Hz, 1 H), 8.88 (dd, 1 H), 8.75 (dd, 1 H), 8.16 (m, 1 H), 8.14–8.10 (m, 1 H), 7.62–7.57 (m, 1 H), 6,88 (d, J = 8.6 Hz, 1 H), 6.68–6.67 (m, 1 H), 4.1–4.09 (m, 4 H), 3.73–3.68 (m, 4 H). **^{13}C NMR** *(126 MHz, d_6-DMSO, ppm)* δ 183.26, 161.69, 161.30, 158.91, 148.05, 146.47, 138.13, 137.61, 135.17, 131.71, 130.98, 129.93, 129.78, 124.29, 124.18, 122.84, 113.74, 107.53, 48.45, 44.20; **FT-IR** (KBr, ν, cm-1): 3439 (N—H…O); 3171 (N—H); 3110−2940 (C—H aromatic); 2940−2750 (C-H, aliphatic); 1728 and 1694 (C═O, imide); 1599 (N═O); 1535 (N—H); 1504 (C═C aromatic).

NIT-7:

Product in the form of a yellow powder, yield: 78 %; mp: 270−273 °C; **^{1}H NMR** *(500 MHz, d_6-DMSO, ppm)* δ 10.54 (s, 1 H), 9.56 (d, J = 2.3 Hz, 1 H), 9.02 (d, J = 2.3 Hz, 1 H), 8.89–8.84 (m, 1 H), 8.75 (dd, 1 H), 8.14–8.10 (m, 1 H), 3.99–3.94 (m, 4 H), 3.73 (dd, 4 H). **^{13}C NMR** *(126 MHz, d_6-DMSO, ppm)* δ 183.60, 161.65, 161.27, 146.46, 137.61, 135.16, 131.70, 130.97, 129.92, 129.77, 124.28, 124.17, 122.82, 66.15, 49.45. **FT-IR** (KBr, ν, cm-1): 3445 (N—H…O); 3252 (N—H); 3110−2940 (C—H, aromatic); 2940−2750 (C—H, aliphatic); 1732 and 1677 (C═O, imide); 1596 (N═O); 1534 (N—H); 1511 (C═C aromatic).

NIT-8:

Product in the form of a yellow powder, yield: 81 %; mp: 258−260 °C; **^{1}H NMR** *(500 MHz, d_6-DMSO, ppm)* δ 10.61 (s, 1 H), 9.58 (d, J = 2.3 Hz, 1 H), 9.03 (d, J = 2.3 Hz, 1 H), 8.88 (dd, 1 H), 8.76 (dd,

1 H), 8.13 (dd, 1 H), 7.12–7.09 (m, 2 H), 7.06–7.02 (m, 2 H), 4.15–4.11 (m, 4 H), 3.27–3.23 (m, 4 H). **^{13}C NMR** *(126 MHz, d_6-DMSO, ppm)* δ 183.26, 161.69, 161.33, 148.03, 146.48, 137.63, 135.18, 131.72, 131.27, 129.94, 124.29, 124.18, 122.84, 117.92, 117.86, 115.96, 115.78, 49.03, 48.80; **FT-IR** (KBr, ν, cm-1): 3497 (N—H…O); 3248 (N—H); 3110−2940 (C—H aromatic); 2940−2750 (C—H aliphatic); 1732 and 1676 (C═O imide); 1596 (N═O); 1537 (N—H); 1507 (C═C, aromatic).

NIT-9:

Product in the form of a yellow powder, yield: 61 %; mp. 254−256 °C; **^{1}H NMR** *(500 MHz, d_6-DMSO, ppm)* δ 10.43 (s, 1 H), 9.57 (d, J = 2.3 Hz, 1 H), 9.02 (d, J = 2.3 Hz, 1 H), 8.88 (dd, 1 H), 8.75 (dd, 1 H), 8.12 (dd, J = 8.2, 7.5 Hz, 1 H), 3.93 (m, 4 H), 2.61 (m, 4 H), 2.32 (m, 1 H), 1.82–1.73 (m, 4 H), 1.60 (d, 1 H), 1.24 (t, J = 9.4 Hz 4 H), 1.11 (m, 1 H). **^{13}C NMR** *(126 MHz, d_6-DMSO, ppm)* δ 182.85, 161.70, 161.31, 146.48, 137.59, 135.14, 131.71, 130.95, 129.93, 129.77, 124.26, 124.18, 62.94, 49.49, 48.66, 28.76, 26.32, 25.76. **FT-IR** (KBr, ν, cm-1): 3424 (N—H…O); 3234 (N—H); 3110−2940 (C—H, aromatic); 2940−2750 (C—H, aliphatic); 1730 and 1682 (C═O, imide); 1598 (N═O); 1538 (N—H); 1511 (C═C aromatic).

The syntheses and characterization of thiosemicarbazides (Tc: 1–10) and corresponding thiosemicarbazones other than NITs (TSC) are presented in supplementary materials.

2.3. Studies of the complexing properties

2.3.1. Studies of the effect of a solvent on chelation

The chelating behavior was tested in various solvents (acetone-***AC***, acetonitrile-***ACN***, methanol-***MeOH***, 0.1 M phosphate buffer-***PBS***) in an equimolar ligand-metal ratio. First, 1 mM salt solutions (chloride cations such as Cu^{2+}, Fe^{3+}) were prepared before use in the following way: appropriate weights of a salt were transferred quantitatively into a 10 mL volumetric flask, which were then filled to the mark with distilled water. Next, the selected compounds (NITs 6, 8, 9 and TSCs 6b, 8e, 9f) were weighed (1 mg) and dissolved in DMSO to obtain a concentration of 1 mM. Then, 0.1 mL of the appropriate cation solution and 0.1 mL of the test compound solution were added into the 10 mL volumetric flask. The flask was supplemented to the mark with various solvents and mixed. The solution was left for four hours, after which the absorbance was measured. The obtained results from the entire series of cations for a given compound were normalized in the same wavelength range to more accurately analyze any changes in the absorption spectrum.

2.3.2. General procedure for the titration

The titration of a compound with Cu^{2+} or Fe^{3+} ions was performed in a MeOH/PBS* (9:1, v/v) system. In the studies, 1 mM solutions of the Cu^{2+} and Fe^{3+} salts and 1 mM solutions of the respective compounds in DMSO (NITs, TSCs, Dp44mT). which had been prepared as described in section 2.3.1, were used. Next, 5 mL of the MeOH/PBS (9:1, v/v) mixture was added to the thirteen volumetric flasks (10 mL). The twelve flasks were divided into two series of six, and the appropriate cation volumes that corresponded to 0.05, 0.1, 0.15, 0.2, 0.3 and 0.4 mL were added to each series (*first series – Cu^{2+} cation, second series – Fe^{3+} ions*). Then, 0.1 mL of the tested compound was added to all thirteen flasks and supplemented with MeOH/PBS (9:1, v/v) to the mark. The prepared solutions were mixed and then allowed to stand for some time. The absorbance was measured two hours after the solutions were prepared. A separate titration series with a metal was preformed according to the above procedure for each compound.

* A 0.1 M solution of PBS, which was obtained by diluting the concentrate in distilled water, in the was used studies.

2.4. Biological studies

2.4.1. Cell cultures

The human colon carcinoma cell line HCT 116 wild type ($p53^{+/+}$) and human breast carcinoma cell line MCF-7 were purchased from the ATCC. The human colon cancer cell line HCT 116 with a p53 deletion ($p53^{-/-}$) was kindly provided by prof. M. Rusin from the Maria Sklodowska-Curie Memorial Cancer Centre and Institute of Oncology in Gliwice, Poland. All of the cell lines were grown as monolayer cultures in 75 cm^2 flasks (Nunc) in Dulbecco's modified Eagle's medium, which was supplemented with 12 % heat-inactivated fetal bovine serum and a mixture of standard antibiotics – 1% v/v of streptomycin and penicillin (all of the reagents were purchased from Sigma-Aldrich). The cells were cultured under standard conditions at 37 °C in a humidified atmosphere at 5% CO_2. Prior to beginning the experiments, all of the cell lines were subjected to routine mycoplasma testing with the specific *Mycoplasma* primers using the PCR technique.

2.4.2. Cytotoxicity studies

The HCT 116 and MCF-7 cells were seeded on 96-well transparent plates (Nunc) at a density of $5{\cdot}10^3$ cells per well and incubated under standard conditions at 37 °C for 24 h. Then, the growth medium was replaced with a medium containing the tested compounds at varying concentrations. The stock solutions of the compounds being investigated were prepared in sterile DMSO. The final concentration of DMSO in the medium did not exceed 0.2 %. After a 72-h incubation with the tested compounds, the media solutions were replaced with 100 µL DMEM (without serum and phenol red) and 20 µL of a CellTiter 96® AQueous One Solution reagent – MTS (Promega) and incubated for 1 h at 37 °C. The absorbance of the samples was measured at 490 nm using a Synergy 4 multi-plate reader (BioTek). The results are expressed as the percentage of the control (untreated cells) and were calculated as the inhibitory concentration (IC_{50}) values using GraphPad Prism 7. Each compound was tested in triplicate in a single experiment with each experiment being repeated at least three times.

2.4.3. Evaluating the chelating ability in vitro – Calcein-AM assay

The HCT 116 and MCF-7 cell lines were seeded into 96-well plates (Black, Clear Bottom, Corning) at a density 10^4 cells/well for 24 h before the experiment. The next day, the growth medium was removed and the cells were washed twice with a serum- and phenol red-free medium (Sigma-Aldrich). Then, the cells were loaded with 20 µM ferric-ammonium citrate (FAC, Sigma-Aldrich) for 4 h and washed three times with a medium without the serum and phenol red. Afterwards, the cells were loaded for 30 min with 0.25 µM of a cell-permeable acetoxymethyl ester of calcein (Calcein-AM, ThermoFisher) and washed three times with the medium (serum- and phenol red-free). The chelators (TSC-10a and Dp44mT) were added at a concentration of 25 µM. Fluorescence intensity (λ_{ex} – 488 nm; λ_{em} – 520 nm) was then conducted for 25 min (measured at intervals of 60 s) at 37 °C using a Synergy 4 multi-plate reader. The results are expressed as the ratio of the maximum fluorescence intensity at each time point (F_n) to the maximum fluorescence intensity in the absence of the chelators (F_0). All of the experiments were repeated three times in triplicate and the results are expressed as the mean ± standard deviation (SD).

3. Results and discussion

3.1. Synthesis and characterization

The presented NIT thiosemicarbazones were synthesized by condensing the selected thiosemicarbazides with 3-nitro-1,8-naphthalic anhydride. This is a new approach for synthesizing TSCs analogues. Fig. 1 shows the structures of the NIT and TSCs (thiosemicarbazones). The synthesis and characterization of the respective novel thiosemicarbazides (Tc) and thiosemicarbazones (TSCs) is described in the supplementary materials. The data for all of the other compounds that were not described here are available in previous publications [12,17,18].

The obtained 3-nitro-1,8-naphthalene thiosemicarbazones were

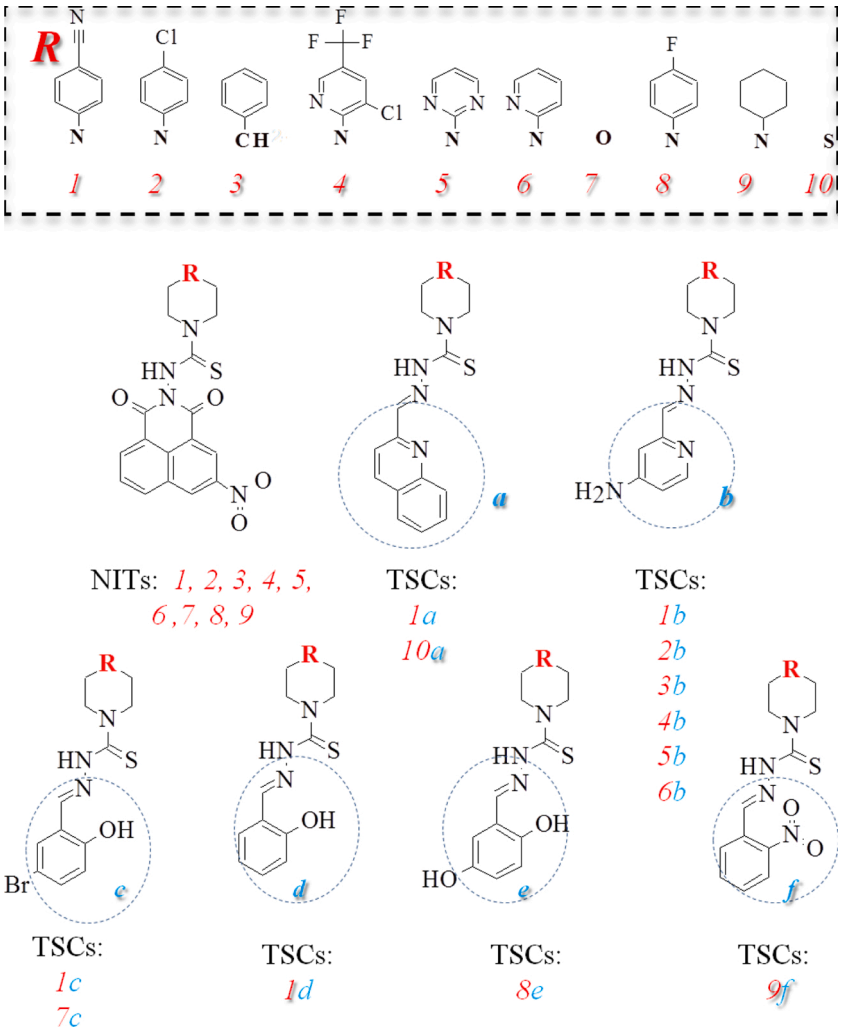

Fig. 1. Structures of the NIT and TSC analogs.

purified by crystallizing them in ethyl acetate. The chemical structure of the obtained compounds was characterized using nuclear magnetic resonance (^{1}H and ^{13}C NMR, COSY and HMQC) and infrared spectroscopy (FTIR). The ^{1}H, ^{13}C NMR and FTIR spectra of all of the compounds are presented in ***Figures S2-S4*** in the ***SI,*** while the characteristic signals that were assigned to the same part of molecules are presented in Fig. 2. The correlation spectra such as COSY and HMQC for NIT-5 in DMSO were used to assign the signals (***Figure S2*** in the ***ESI***). A single signal in the range of δH 10.43–10.61 ppm in the ^{1}H spectrum indicates the presence of a H–N proton (a secondary amine). This proton is connected to a nitrogen atom (secondary amine) as was indicated by the COSY spectrum. Furthermore, a lack of a correlation with the carbon atom in the HMQC spectrum was also revealed. The high displacement values may indicate the occurrence of a hydrogen bond between N—H··· O=C in the imide group (***Figure S3*** in the ***ESI***). The presence of hydrogen bonds was confirmed by the FTIR spectrum, in which a band in the range of 3320−3654 cm^{-1} occurred.

Based on the COSY and HMQC spectra, the signals from the protons (^{1}H) and carbons (^{13}C) could be precisely assigned to the structure of the compounds. The signals in the rangers: ***(a)*** 9.58−9.56 ppm, ***(b)*** 9.04−9.02, ***(c*** and ***e)*** 8.88−8.87 and 8.77−8.74 ppm and ***(d)*** 8.12−8.12 ppm were assigned to the five protons in the aromatic ring of naphthalimide (***Figures S2- S3*** in the ***ESI)***. Similarly, the signals of the ten carbon atoms were assigned as follows (***Figures S2*** and ***S4*** in the ***ESI):*** ***(3)*** *146.45–146.49 ppm,* (***6*** and ***8)*** *137.59–137.63* and *135.18−135.14 ppm,* (***2)*** *131.70–131.72 ppm,* ***(7)*** *131.00−130.95 ppm,*

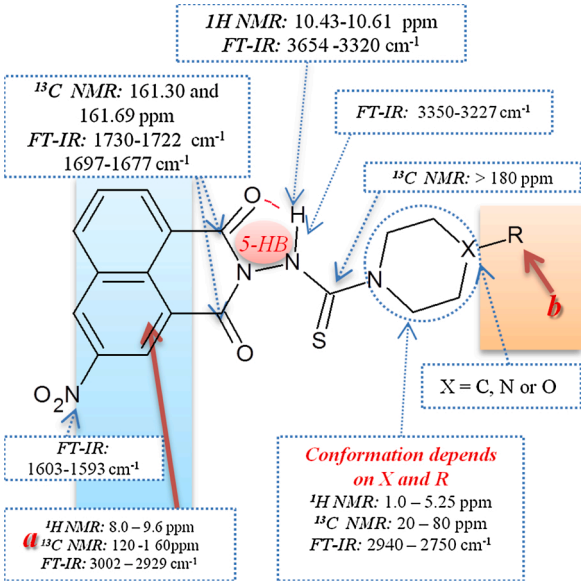

Fig. 2. The characteristic signals (^{1}H, ^{13}C, FTIR) that were assigned from the same parts of molecules.

(***1*** and ***9)*** *129.95–129.92* and *129.79–129.77 ppm,* (***5*** and ***10)*** *124.30–124.26* and *124.23–124.15 ppm* and (***4***) *122.90–122.81 ppm*. The other signals that are typical for the aromatic range in both the ^{1}H and ^{13}C NMR spectra originated from the group that was attached to the six-membered imide ring. In addition, a signal above 180 ppm corresponding to the group C═S was visible in all of the ^{13}C spectra. A characteristic signal for the carbon in nitrile group at 89.61 ppm that is typical for the absorption of CN at 2213 cm^{-1} was detected in the ^{13}C NMR and FTIR spectra of the NITs-1 compound. The type of atom (X═N, C or O) as well as the substituent (R) influenced the conformation in the six-membered saturated heterocyclic, e.g. the piperazine [27], morpholine [28] or piperidine [29–31] ring. Molecules that have heterocyclic rings usually adopt chair conformations (lowest energy) but with a different axial or equatorial position of the substituent (Fig. 3).

3.2. Optimizing the compound structures

The theoretical calculations were performed using the density functional theory (DFT) and were carried out using the Gaussian09 program [33] on the B3LYP/6−31g++ level [34,35]. The molecular geometry of the singlet ground state of the compounds was optimized in the gas phase and its electronic structures and electronic transitions were calculated using the Polarizable Continuum Model (PCM) with methanol as the solvent. Such calculations were carried out to analyze the structure of the frontier molecular orbitals and energy levels and the UV–vis data. The optimized geometries of the compounds are depicted in ***Figures S5*** and ***S6*** in the Supplementary Information, which presents the experimental and calculated IR spectra. The piperidine (NIT-3), morpholine (NIT-7) and piperazine (for all others) fragments had a chair conformation. The geometrical parameters of the amine N—H and amide carbonyl group indicated the possibility of a hydrogen bond with a H···O distance 2.3–2.4 Å and an N—H…O angle in the range of 96°-101°. A second intramolecular hydrogen bond is possible between C═S and piperazine, morpholine or piperidine C—H with a distance 2.5 Å and a C—H…S angle close to 113°. The calculated hydrogen bond vibrations corresponded to the experimental data well as can be seen in ***Figure S7***. The frontier molecular orbitals of the compounds were characterized based on the optimized geometries. In order to obtain a detailed description of the molecular orbitals, the contribution of the parts, i.e. 3-nitro-naphthalene, HN-CS- and substituted six-membered saturated ring fragments to a molecular orbital, were calculated. The obtained DOS diagrams are depicted in ***Figure S8*** and the composition of the selected molecular orbitals in the ground state are listed in **Table S1** in the ***ESI***. The electronic structures of the compounds were similar and LUMO in each case was localized on the 3-nitro-naphthalene part, and therefore the changes in the energy of this level were negligible. The HN-CS- fragment played a dominant role in the HOMO of NITs-3 and NITs-7, that is, in the case of the compounds in which the six-membered saturated heterocyclic ring was substituted with piperidine or, as in the case of NIT-7, unsubstituted morpholine. In other cases, the HOMO was localized on the substituent of the six-membered saturated ring with the exception of NIT-4 where the share of HN-CS- was significant. The thiosemicarbazide (HN-CS-) part played a dominant role in the H-1 to H-5 levels, which is important for interpreting the lowest energy band on the UV–vis spectra. In the energy range that corresponded to the first, lowest energy, the band on the electronic absorption spectrum was calculated H-2/3 → LUMO transitions, which corresponded to the excitation between the nonbonding orbitals that were localized on the S═C-(saturated six-membered ring) and 3-nitro-naphthalene.

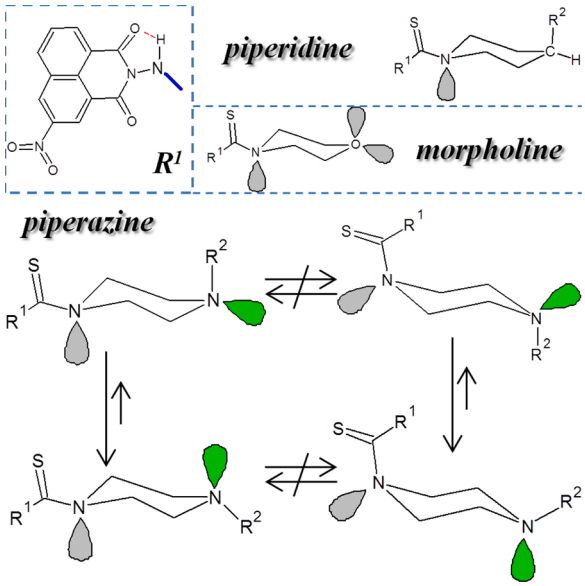

Fig. 3. Possible conformers and their interchange [28,31,32].

3.3. Complexing the properties of the compounds

The ability to complex Cu^{2+} or Fe^{3+} ions may prove to be the key to explaining the cytotoxicity of drugs [1]. Therefore, we decided to measure and analyze the complexing properties of the tested compounds. First, the influence of the solvent such as acetone (AC), acetonitrile (ACN), methanol (MeOH) and 0.1 M PBS on the complexation was investigated for the selected compounds (NITs 6, 8, 9 and TSCs 6b, 8e, 9f) at an equimolar ratio of thiosemicarbazone and metal (***Figure S9*** in the ***ESI***). These studies revealed that the PBS solution significantly affected the Cu^{2+} complexation by TSC-6b and TSC-8e, and to a small extent, on the Fe^{3+} complexation by TSC-8e. On the other hand, methanol had a beneficial effect on the complexation of both the Cu^{2+} and Fe^{3+} ions. It was also observed that TSC-6b and TSC-8e had a good affinity for the Cu^{2+} ions, which was slightly weaker for Fe^{3+}, whereas the complexing properties of TSC-9f, NIT-6, NIT-8 and NIT-9 were negligible. In our spectroscopic experiments, phosphate buffered saline was used to reflect the environment of a biological system.

However, it appears that the presence of the phosphate groups in a PBS buffer may have a significant impact on the binding of metal ions and other molecules as has been presented in few reports [36–38]. However, the influence of the other solvents (AC, ACN) on complexation was insignificant, and therefore, they were omitted in the following part. These data may suggest that the complexation of metals by the tested TSCs are dependent on the character of the solvent as the effect was more visible in the polar protic solvent – methanol. Based on these results, further studies were performed of the complexing properties in the MeOH/PBS (9:1, v/v) system. In this way, we limited the possible interactions of the sodium phosphates with metal ions, which may affect the final results of TSC experiments with complexing metal ions in a solution. Thus, these studies will allow the ability of the compounds to complex Cu^{2+} or Fe^{3+} ions to be compared and their biological properties to be discussed. For this purpose, the metal titration (5−40 μM) of the compounds was performed in the MeOH/PBS (9:1, v/v) system. The superimposed spectra of the spectroscopic changes that were caused by the addition of various amounts ions is presented in Figs. 4 and 5 and ***Figures S10 - S11***. Furthermore, the changes that resulted from the addition of an equimolar amount of a metal for all of the compounds tested is presented in ***Figures S12 to S14***, whereas the spectroscopic data are collected in Table 1.

Two characteristic bands are visible in the UV–vis spectrum for the pure compounds (***blue line***). The first band in the range of 240–300 nm corresponds to the part thiosemicarbazone (C═S) with an unsaturated six-membered ring, while the second band in the range from 300 to 400 nm could have been caused by the n-π* transitions in the substituent *a–f* (Fig. 1, derivatives of pyridine, quinoline or aryls) [39] or in the imide unit [40–42] (*see* Table 1.). Importantly, observing changes in these regions may enable to localize the site of Cu^{2+} or Fe^{3+} ions

Table 1
The spectroscopic data of tested compounds and its complexes with Cu(II) or Fe(III).

code	Compounds	Cu(II)-complex (1:1)		L:Cu*	Fe(III)-complex (1:1)		L:Fe*
	λ_{max} [nm]	λ_{max} [nm]	Isosbestic point [nm]		λ_{max} [nm]	Isosbestic point [nm]	
NIT-1	284, 330***sh***	–	–	–	–	–	–
TSC-1a	290, 350	296, 360, 453	363	1:1	290, 360, 417	368	1:1
TSC-1b	290, 370	297, 448	335, 395	1:1.5	294, 432, 490***sh***	337, 390	1:1.5
TSC-1c	295, 341	294, 330***sh***,402	307, 339, 353	1:1.5	295, 385***sh***	–	–
TSC-1d	294, 335***sh***	295, 327***sh***,392	308, 343	1:1.5	294, 377***sh***	–	–
NIT-2	280***sh***, 328	–	–	–	–	–	–
TSC-2b	256, 370	256, 294, 370, 448	283, 335, 396	1:1.5	256, 380, 440, 490***sh***	288, 335, 392	1:1.5
NIT-3	278***sh***, 330	–	–	–	–	–	–
TSC-3b	264, 373	295, 377, 450	282, 336, 396	1:1.5	309, 430, 490^{sh}	288, 338, 390	1:1
NIT-4	272, 328	–	–	–	–	–	–
TSC-4b	267, 372	270, 297***sh***, 375, 446	286, 336, 395	1:2	266, 308***sh***, 381, 450***sh***, 490***sh***	288, 337, 391	1:1.5
NIT-5	278, 328	–	–	–	–	–	–
TSC-5b	283***sh***, 373	290, 373, 450	283, 336, 397	1:1.5	308, 383, 440***sh***, 490^{sh}	289, 337, 393	1:1.5
NIT-6	280, 328	–	–	–	–	–	–
TSC-6b	296***sh***, 371	300, 451	289, 328, 400	1:1.5	304, 437, 492^{sh}	296, 344, 394	1:1.5
NIT-7	278, 328	–	–	–	–	–	–
TSC-7c	284, 339	280, 329, 402	267, 306, 340, 354	1:1.5	281, 337, 388	–	1:4**
NIT-8	277, 330	–	–	–	–	–	–
TSC-8e	279, 330	324, 347, 375, 392^{sh}	276, 310, 347	1:1.5	306, 364	–	–
NIT-9	284***sh***, 328	–	–	–	–	–	–
TSC-9f	295, 345***sh***	308, 390^{sh}	–	–	–	–	–
TSC-10a	286, 312, 337, 352***sh***	289***sh***, 312, 378, 445	–	1:3	286, 312, 337, 352***sh***, 422	–	1:4**

Medium: MeOH:PBS (9:1, v/v); c = 10^{-5} mol/dm^3; ***sh***-shoulder; *- maximum L: Me ratio above which there were no visible changes in the spectrum, determined on the basis of the UV–vis spectra titration with metals, presented in Fig. 4 and Figures S10 and S11 in ESI; **- studies were not conducted above this L: Me ratio (1: 4).

complexation by compounds to be determined. Moreover, the changes in absorption spectra as well as forming of isosbestic points caused by complexation of Cu(II) and Fe(III) ions are clearly seen. It can be noticed that the isosbestic points are located at similar values (irrespective of R substituent or the type of cation), e.g. for derivatives with 3-aminopyridine (TSC: 2b, 3b, 4b, 5b, 6b) points occur at ≈ 290, 335 and 395 nm (*see* Table 1). In addition, the superimposed UV–vis spectra of metals titration was used to determine ratio of ligand: metal and the corresponding values are shown in Table 1. The ligand to metal ratio in most of the examples is 1: 1.5, which indicates the possibility of forming cluster complexes [43], for example complex consists of of 2 ligands and a 3 metal center to form the [M_3L_2] model [44,45]. The formation of such systems may be favored by additional donor centers present in the structure of six-membered saturated heterocyclic [46]. In Fig. 4, the results from the metal titration are presented taking into account the effect of the different substituents (*NITs and b, e, f* as show in Fig. 1) on the ability to form complexes. We observed that the TSC-6b and TSC-8e had the ability to form complexes with Cu^{2+} and Fe^{3+} ions in contrast to TSC-9f. This is due to the presence of the pyridine (TSC-6b) and hydroxyl (TSC -8e) groups in these molecules. It was found that the presence of the nitro group (TSC-9f, NIT-6, NIT-8 and NIT-9) limited the complexing ability. In addition, ***Figure S13*** presents the superimposed spectra of the compounds that contained the (4-cyanophenyl)piperazine unit (TSC: 1a, 1b, 1c, 1d, NIT-1) relative to the Cu^{2+} and Fe^{3+} ions at an equimolar ratio. The clearly visible spectral changes, which were associated with the Cu^{2+} and Fe^{3+} complexation, can be identified for TSCs: 1a and 1b, i.e. the compounds that contain nitrogen within the ring.

However, the changes in the spectra for the compounds that have the −OH group (TSC: 1c, 1d) indicated that chelation mainly involved Cu^{2+}. In turn, the Fe^{3+} complexation was less visible than in the case of the heteroaryl derivatives. Whereas, the compounds that had the 3-nitro-1,8-naphthalene (NITs) substitution did not show any spectroscopic transformations, thereby indicating a lack of complexing ability against Cu^{2+} and Fe^{3+}. A comparison of the studied TSCs and NITs indicated that the latter lacked of a complexing ability, which may be attributed to the steric hindrance within the large naphthalimide unit. The results for NITs 2, 3, 4, 5, 6 compared to the TSC with 3-aminopyridine group are presented in Figure S12 in the ESI, additionally they confirm it. Due to the visible difference in the complexing ability of the Fe(III) ions by thiosemicarbazones (TSC), the further part of this work focuses on explaining this relationship.

Thiosemicarbazones with metals, depending on the structure and number of ligands (L), generally can form mono- or bis- complexes [47]. In these systems, the complexation occurs through a sulfur atom, nitrogen (imine) and nitrogen atoms present in quinoline or 3-aminopyridine [48]. Whereas, in derivatives with a 2-hydroxyphenyl group, the complexation may occur via an oxygen atom [49].

Therefore, the TSCs coordinate the cation by means of N (imine), S and when an additional coordinating group is present (O, N) may include the typical tridentate coordination fashion (Fig. 5a). Moreover, it was shown that the Fe(III) forms high stable mono and bis complexes with Triapine bearing the well-known ($N_{pyridine}$, N, S^-) coordination mode and $[Fe(III)L_2]^+$ predominates at pH 7.4 [50]. Moreover, for derivatives with salicyl aldehye unit at pH = 7.4 species $[Fe(III)L_2]^-$ are predominated [39]. As shown by recent studies the method binding of the metal cations by the third atom (O or N) may be crucial for the properties of the metal-complex. On the example of cobalt complexes, greater catalytic activity of the complex with the pyridine group than with the quinoline group was proved, pointing to the important roles of both the electronic and steric effects of a substituent. Moreover, a correlation between the basicity of nitrogen in aromatic amines (pyridine, quinoline, isoquinoline) and the N-Metal bond length was described on the example of complexes with cobalt ions [51]. In addition, in the use of gold complexes, the influence of the pyridine substituent in complex on catalytic properties was noticed, which was directly related to the different coordination ability of the pyridine and quinoline nitrogen atoms. Based on these studies, selective coordination of pyridine nitrogen, whereas quinoline nitrogen atoms failed to undergo complexation was found [52]. Based on those reports we analyzed the effect of the substituent (pyridine, quinoline, 2-hydroksyfenol) at the imino bond on the ability of complexing iron (Fig. 5). Basicity of nitrogen atom in pure 3-aminopyridine (pKa = 5.98) is higher than in quinoline (pKa = 4.85) [53,54]. Moreover, the calculated pKa values of imine nitrogen show the reduction of the basicity of the imine nitrogen in series TSC-1b (13.32) > TSC-1a (12.77) > TSC-1c (9.44) (ESI section 1.3). Thus, it is expected that higher basicity of nitrogen atoms (N_{imine}, N_{Ar}) for TSC-1b favor the formation of a more stable iron complex than for TSC-1a or TSC-1c (Fig. 5). Analyzing Fig. 5 for the TSC-1b derivative, the changes as the

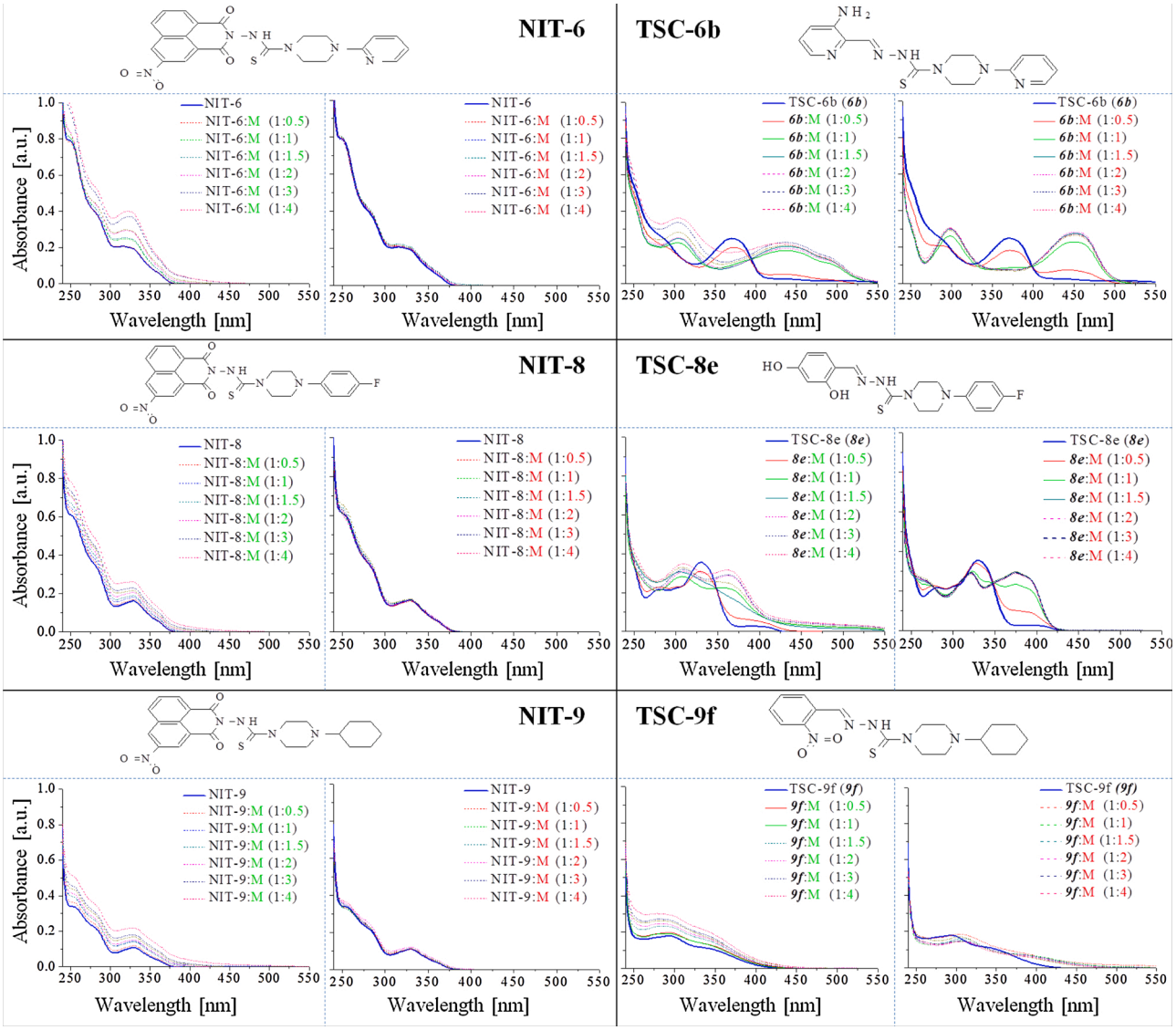

Fig. 4. UV–vis absorption titration spectra of the investigated compounds (10 μM) with Fe^{3+} (**M**) and Cu^{2+} (**M**) (5-40 μM) in a MeOH/PBS (9:1, v/v) mixture at room temperature two hours after it had been prepared.

amount of iron increases include the complete reduction of the band in the range of 325–380 nm and the formation of the new band in the range of 400 to 550 nm with the maximum absorption at 432 nm and the shoulder at 490 nm. Thus, changes in this range are evident for each derivative with 3-aminopyridine (Fig. S10-S11), which is probably related to the better complexation of iron ions by the more basic nitrogen atoms. Whereas, in the case of TSC-1a, the changes in the UV–vis spectrum include the partial reduction of the band in the range 320−370 nm (with $\lambda_{max} = 350$ nm) and the formation a new band in the range 375−500 nm. It can be seen that the band with $\lambda_{max} = 350$ nm does not disappear completely. We can suppose that the result of a weaker interaction nitrogen atoms with iron ion, as was in the case with the Co(II) [51] or Au(III) [52] complexes. In the third case, for a TSC-1c derivative with a 2-hydroxyphenyl group, the changes in the spectrum include slight increase of the band in the range of 330–420 nm without distinct shaping of the λ_{max}. The main reason for such changes may be steric hindrance which may reduce the possibility of complexing iron ions. Other TSC derivatives with hydroxyl or nitro groups (1c, 1d, 7c, 8e, 9f) had a weaker or no ability to coordinate the Fe^{3+} ions. The above considerations were supplemented with DFT calculations. The bonding properties and energy analysis were made for the Fe-thiosemicarbazone complexes $[ML_2]$. The Wiberg indices and the bond distances of Fe-L are similar in the complexes to provide descriptions of ligands bonding in the complexes the fragmentation model according to the energy deposition (EDA) scheme was chosen (cf. ESI Tables 2–4). The calculated interaction energies collected in Table S4 and the total energy ΔE_{int} is mainly determined by the TSC ligand. Only in the case of Fe-Tsc-1b the ΔE_{elect} and ΔE_{Pauli} components compensate each other and the repulsive term has a significant advantage over the electrostatic interaction. This indicates that the $[FeL_2]^{+} \rightarrow [FeL]^{2+} + L^{-}$ process is not preferable. The total attractive interactions $\Delta E_{elect} + \Delta E_{orb}$ are rather high and play a meaningful role in the binding interactions in Fe-TSC-1b and TSC-1a complexes. In the case of Fe-Tsc-1c compound the attractive component is practically compensated by repulsion factor so the stability of this compound is small. Moreover, the calculated steric factor contained in ΔE_{Pauli} (ESI Table 4) is the highest for the Fe-TSC-1c and confirms the above statement.

The TSC analogs, which are presented in ***Figure S10 and S11***, show the pronounced changes in a spectrum in the range of 220−250 nm, especially in the complexation of Cu^{2+} ions. Therefore, in the next part, we analyzed the impact of the unsaturated six-membered ring in the TSC on metal ion complexation. The analysis for the compounds that

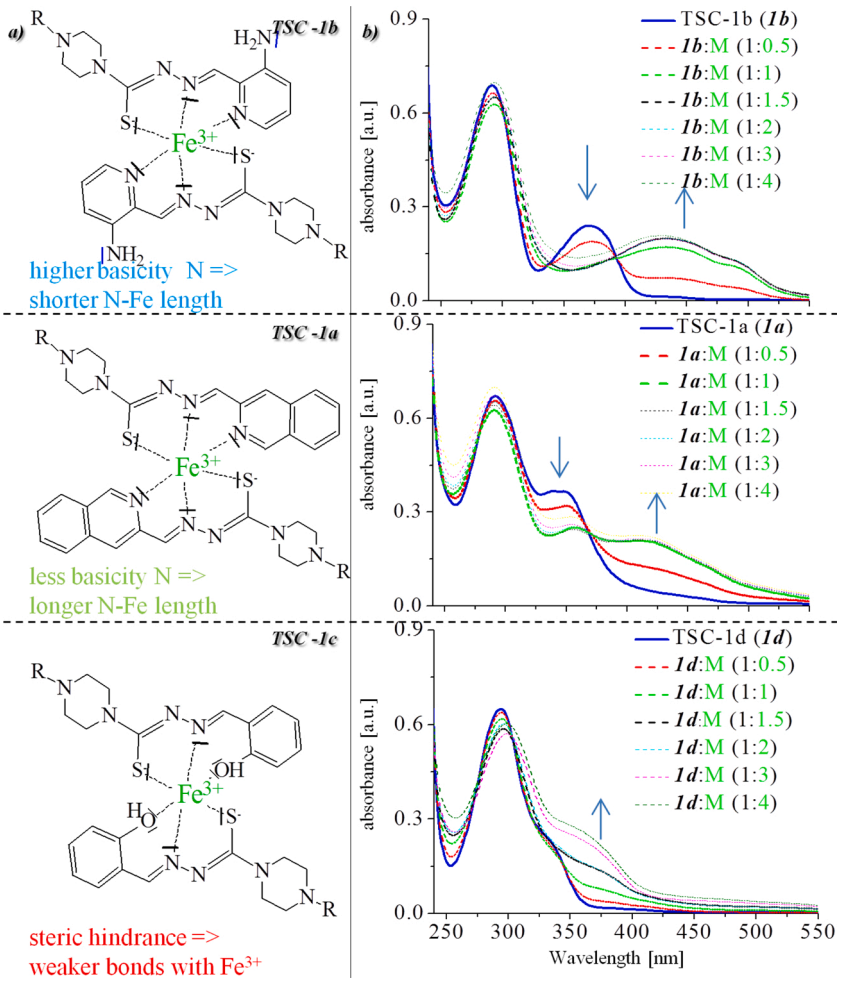

Fig. 5. a) The proposed model of iron cation binding on the example of a [FeL_2] complex, including ligands: Tsc - 1a, 1b, 1c by neutral pH and R = 4-cyanophenyl group; **b)** UV–vis absorption titration spectra of the investigated compounds (10 μM) with Fe^{3+} (5-40 μM) in a MeOH/PBS (9:1, v/v) mixture.

contained pyridine, piperazine, morpholine and thiomorpholine is presented in ***Figure S11***. It was found that the type of substitution (by a donor atom: N, O, S or C) did not significantly affect the chelation ability. Based on this, we can conclude that the second heteroatom (next to nitrogen at the para position) in the unsaturated six-membered ring does not participate in copper or iron complexation. On the other hand, it was observed that the TSCs with both a heteroaryl and an −OH group chelated the Cu^{2+} ions easily. This was visible for each substituent on the imine bond (Figs. 4 and ***S10-S11***). In addition, for the Cu^{2+} chelation, changes that ranged from 240–300 nm were observed, which indicates a complexation between Cu^{2+} and —C═S and the adjacent nitrogen atom. No similar effect was observed for the Fe^{3+} chelation. Moreover, the o-hydroxyphenyl imines are known for their good copper chelation properties [55–57]. Although the unsaturated six-membered ring did not create the coordination band with metal, it undoubtedly had an impact on the biological activity that affected the lipophilicity or other specific interactions with a receptor. In our previous *in vitro* studies, we showed that highly active thiosemicarbazone derivatives have a better chelation ability to form complexes with Cu^{2+}, which correlated well to their therapeutic response [12,17]. This corresponds to the results of Stacy et al. who demonstrated that the complexes Dp44mT with copper can generate larger amounts of ROS, which induces a Pgp-dependent lysosomal membrane permeabilization, thereby increasing cytotoxicity and overcoming multi-drug resistance [57]. Additionally, it should not be forgotten that Cu^{2+} chelation by TSCs is a complex phenomenon that involves ionophoric effects, i.e. the ability to transport metal ions through the cell membranes. This intrinsic mechanism of TSCs enables the concentration of metal in the cellular environment to be increased, which causes a disturbance of cell homeostasis and its damage.

3.4. Anticancer activity

The results of the anticancer antiproliferative activity of the studied compounds are presented in Table 2. We performed cytotoxicity assays against two human colon cancer cell lines: the wild type (HCT 116 $p53^{+/+}$) and negative p53 (HCT 116 $p53^{-/-}$) and the human breast cancer cell line (MCF-7). The selection of those cell lines was related to the fact that colon and breast tumors are characterized by an increased iron uptake, cell metabolism and sensitivity to redox changes. Generally, all of the tested TSCs had a strong or weak activity, while NITs were inactive against all of the cancer cell lines. This corresponds well to the chelating ability of the tested TSCs and NITs. The aminopyridine derivative TSC-2b had the highest activity among the tested compounds (the IC_{50} values were 0.14 μM for HCT 116 $p53^{+/+}$ and 0.20 μM for MCF-7). In addition, it is worth noting that the TSCs with the aminopyridine substituent (TSCs 1b, 3b, 4b, 5b, 6b) also had a excellent activity with IC_{50} values that ranged from 0.14 μM to 1.9 μM for both of the HCT 116 cell lines. Apparently, a good activity of the aminopyridines correlates with the better chelation ability of the Fe^{3+} ions as was observed in the spectroscopic studies (Figs. 4 and 5). The rest of the TSCs had low activity values of IC_{50} in the range of 7.76 μM to 20.43 μM for the HCT 116 cells. The exceptions were TSC-1a and TSC-1c, which had a good/moderate activity. There was similar trend for the MCF-7 cells, which was consistent with the spectroscopic analysis of the Fe^{3+} chelation.

Table 2
Anticancer properties of the tested compounds (NITs and TSCs) against the human colon and breast cell lines.

Compounds	*Cytotoxicity [μM]*		
	HCT 116 p53+/+	*HCT 116 p53−/−*	*MCF-7*
NIT-1	>25	>25	>25
TSC-1a*	0.56 ± 0.14	0.43 ± 0.03	0.23 ± 0.11
TSC-1b*	1.45 ± 0.45	0.75 ± 0.35	3.81 ± 1.02
TSC-1c	5.30 ± 1.33	1.41 ± 0.43	3.33 ± 0.38
TSC-1d	15.87 ± 5.97	8.33 ± 1.37	9.98 ± 1.61
NIT-2	>25	>25	>25
TSC-2b*	0.12 ± 0.01	0.17 ± 0.02	0.20 ± 0.05
NIT-3	>25	>25	>25
TSC-3b	0.14 ± 0.02	0.28 ± 0.01	0.23 ± 0.04
NIT-4	>25	>25	>25
TSC-4b*	0.17 ± 0.02	0.16 ± 0.01	0.26 ± 0.04
NIT-5	>25	>25	>25
TSC-5b*	0.67 ± 0.05	0.65 ± 0.06	1.73 ± 0.39
NIT-6	>25	>25	>25
TSC-6b*	1.90 ± 0.29	0.14 ± 0.02	1.12 ± 0.11
NIT-7	>25	>25	>25
TSC-7c	19.24 ± 2.94	7.76 ± 1.57	16.55 ± 1.04
NIT-8	>25	>25	>25
TSC-8e	11.36 ± 4.69	9.37 ± 0.65	>25
NIT-9	>25	>25	>25
TSC-9f*	11.78 ± 3.28	20.43 ± 2.29	>25
TSC-10a*	18.31 ± 0.92	5.85 ± 0.45	>25
Dp44mT	$1.23{\cdot}10^{-3}$ ± $0.18{\cdot}10^{-3}$	$1.10{\cdot}10^{-3}$ ± $0.06{\cdot}10^{-3}$	$1.14{\cdot}10^{-3}$ ± $0.40{\cdot}10^{-3}$

The structures of the tested compounds are presented in Fig. 1.
* The compound described in the publication: TSC-1a [12]; TSC: 1b, 2b, 4b, 5b, 6b [18] and TSC: 9f, 10a [58].

In the next step, we examined the ability of the TSCs to complex the iron ion at the cellular level. For the intracellular iron binding assay, which is based on a measurement of the calcein fluorescence intensity, we selected two derivatives: the highly active – Dp44mT and the moderately active – TSC-10a. As is presented in Fig. 6, there was a significant increase in the calcein fluorescence after the Dp44mT treatment. This effect may have been associated with a decrease in the labile iron pool, which confirms the high efficiency of the intracellular iron chelation of Dp44mT on both cell lines. On the other hand, as was expected, a much smaller effect was observed for TSC-10a. In addition, the small differences in the fluorescence intensity that was observed between the tested cell lines appear to correlate with the anticancer activity of TSC-10a (IC_{50}: 18.31 μM for HCT 116 $p53^{+/+}$ and more than 25 μM for MCF-7). These observations confirm the overall relationship between the anticancer activity and chelating properties of the TSCs. Importantly, similar dependences were recorded in our previous studies on uptake and mobilization of iron from cells [16,59]. In general, we indicated that the TSCs that are based on the di-2-pyridine ketone moieties had better ability to bind cellular Fe^{3+} than their quinoline analogs. In turn, this could be correlated with the improvement of the cytotoxicity of the corresponding compounds. An interesting example was the quinoline derivative that had been substituted with a morpholine ring, which was characterized by both a weak anticancer activity and the ability to mobilize cellular iron compared to its 8-hydroxyquinoline analog that had a high anticancer potency [16,60].

4. Conclusion

A broad study of the chelating behavior of a series of TSCs and NITs compounds demonstrated that the efficient complexing of Cu^{2+} and Fe^{3+} ions has a significant influence on the biological activity of the tested compounds. Because metal ions play an important role in the cellular processes, a disturbance in their natural homeostasis has a critical impact on a cell. In this work, we did an in-depth analysis of the chelating behavior of nine newly synthesized derivatives of NITs and TSC analogs. The synthetic pathway of the NITs is presented here for the first time. Detailed spectroscopic analyses in different solvents and conditions involving Cu^{2+} and Fe^{3+} ions permitted a comprehensive determination of the structural features that influence the complexation properties. Based on the UV–vis spectra titration with Fe^{3+} and theoretical calculations, the chelating ability for the TSC derivatives was analyzed. The stability of Fe(III)-complexes depends on the basicity of nitrogen atoms in the analyzed compounds. Therefore, the drivatives containing 3-aminopyridine may form more stable complexes with Fe^{3+} ions than with the quinoline substituent. In the case of derivatives in the hydroxyl group, steric hindrance and lower basicity of N_{imine} may affect the low stability of the complex with Fe^{3+} ions. Biological studies of the cytotoxicity on three cancer cell lines showed that the binding of metal ions is crucial for the anticancer activity of the tested compounds. The formation of a coordination bond with metal depends on an advantageous arrangement of the donor atoms.

Author's contribution

RRK – Methodology, Validation, Investigation, Visualization, ***KM*** – Methodology, Validation, Writing, ***RG*** – Methodology, Investigation, Visualization, ***AMW*** – Conceptualization, Formal analysis, Writing , ***JGM*** –Methodology, Formal analysis, Writing, ***ESB*** – Formal analysis, Writing - Review & Editing, ***MK*** – Methodology, Conceptualization, Validation, Formal analysis, Writing, Visualization, ***JP***

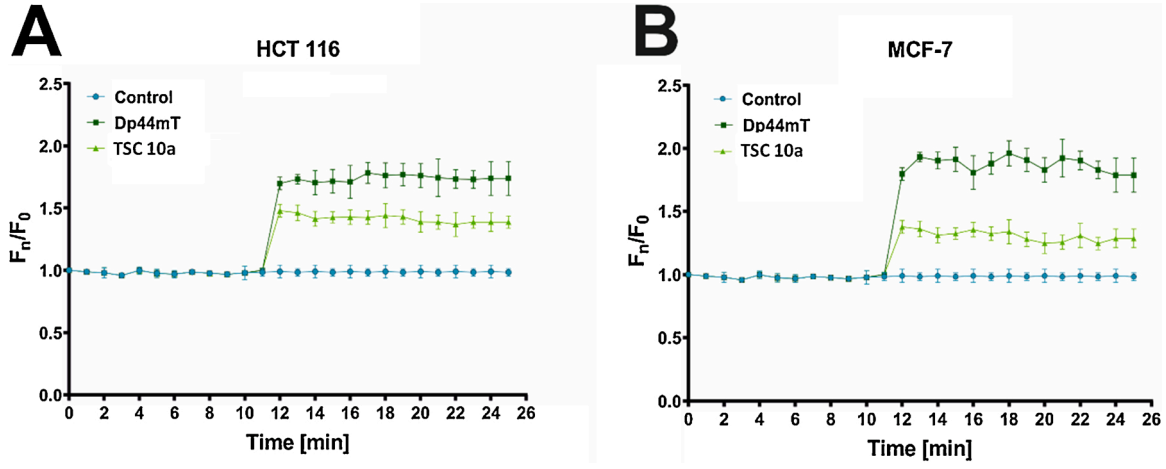

Fig. 6. The intracellular chelating properties of Dp44mT and TSC-10a (25 μM) after FAC (20 μM) loading in the HCT 116 (A) and MCF-7 (B) cell lines. Cells that had not been treated with chelators were the control. The chelators were administered in the 10th minute of the measurement.

–Conceptualization, Writing - Review & Editing.

Declaration of Competing Interest

The authors declare that they have no known competing financial interests or personal relationships that could have appeared to influence the work reported in this paper.

Appendix A. Supplementary data

Supplementary material related to this article can be found, in the online version, at doi:https://doi.org/10.1016/j.jphotochem.2021.113314.

References

[1] Y. Yu, J. Wong, D.B. Lovejoy, D.S. Kalinowski, D.R. Richardson, Chelators at the Cancer coalface: desferrioxamine to triapine and beyond, Clin. Cancer Res. 12 (2006) 6876–6883.

[2] P. Heffeter, V.F.S. Pape, É.A. Enyedy, B.K. Keppler, G. Szakacs, Ch.R. Kowol, Anticancer thiosemicarbazones: chemical properties, interaction with Iron metabolism, and resistance development, Antioxid. Redox Signal. 30 (2019) 1062–1082.

[3] R.R. Kumar, R. Ramesh, J.G. Małecki, Ru(II) carbazole thiosemicarbazone complexes with four membered chelate ring: synthesis, molecular structures and evaluation of biological activities, J. Photochem. Photobiol. B, Biol. 165 (2016) 310–327.

[4] C. Santini, M. Pellei, V. Gandin, M. Porchia, F. Tisato, C. Marzano, Advances in copper complexes as anticancer agents, Chem. Rev. 114 (2014) 815–862.

[5] R. Jawaria, M. Hussain, H.B. Ahmad, M. Ashraf, S. Hussain, M.M. Naseer, M. Khalid, M.A. Hussain, M. al-Rashida, M.N. Tahir, S. Asim, Probing ferrocene-based thiosemicarbazones and their transition metal complexes as cholinesterase inhibitors, Inorg. Chim. Acta Rev. 508 (2020) 119658.

[6] H. Pervez, N. Khan, J. Iqbal, S. Zaib, M. Yaqub, M.M. Naseer, Synthesis and in vitro bio-activity evaluation of N 4-benzyl substituted 5-Chloroisatin-3-thiosemicarbazones as urease and glycation inhibitors, Acta Chim. Slov. 65 (2018) 108–118.

[7] H. Pervez, N. Khan, J. Iqbal, S. Zaib, M. Yaqub, M.N. Tahir, M.M. Naseer, Synthesis, crystal structure, molecular docking studies and bio-evaluation of some N^4-benzyl-substituted isatin-3-thiosemicarbazones as urease and glycation inhibitors, Heterocyclic. Commun. 24 (2018) 51–58.

[8] H. Pervez, N. Khan, S. Zaib, M. Yaqub, M.M. Naseer, M.N. Tahir, J. Iqbal, Synthesis, X-ray molecular structure, biological evaluation andmolecular docking studies of some N4-benzyl substituted 5-nitroisatin-3-thiosemicarbazones, Bioorg. Med. Chem. 25 (2017) 1022–1029.

[9] K. Gaur, A.M. Vázquez-Salgado, G. Duran-Camacho, I. Dominguez-Martinez, J. A. Benjamín-Rivera, L. Fernández-Vega, L.C. Sarabia, A.C. García, M. Vega-Cartagena, S.A. Loza-Rosas, X.R. Acevedo, A.D. Tinoco, Iron and copper intracellular chelation as an anticancer drug strategy, Inorganics. 6 (2018) 126–163.

[10] M.E. Helsel, K.J. Franz, Pharmacological activity of metal binding agents that alter copper bioavailability, Dalton Trans. 44 (2015) 8760–8770.

[11] Y. Yu, D.S. Kalinowski, Z. Kovacevic, A.R. Siafakas, P.J. Jansson, Ch. Stefani, D. B. Lovejoy, P.C. Sharpe, P.V. Bernhardt, D.R. Richardson, Thiosemicarbazones from the Old to New: Iron Chelators That Are More Than Just Ribonucleotide, J. Med. Chem. 52 (2009) 5271–5294.

[12] A. Mrozek-Wilczkiewicz, K. Malarz, M. Rejmund, J. Polanski, R. Musiol, Anticancer activity of the thiosemicarbazones that are based on di-2-pyridine ketone and quinoline moiety, Eur. J. Med. Chem. 171 (2019) 180–194.

[13] Ch. Stefani, G. Punnia-Moorthy, D.B. Lovejoy, P.J. Jansson, D.S. Kalinowski, P. C. Sharpe, P.V. Bernhardt, D.R. Richardson, Halogenated 2′-Benzoylpyridine thiosemicarbazone (XBpT) chelators with potent and selective anti-neoplastic activity: relationship to intracellular redox activity, J. Med. Chem. 54 (2011) 6936–6948.

[14] D.S. Kalinowski, P. Quach, D.R. Richardson, Thiosemicarbazones: the new wave in cancer treatment, Future Med. Chem. 6 (2009) 1143–1151.

[15] J. Denga, P. Yua, Z. Zhanga, J. Wanga, J. Caib, N. Wua, H. Suna, H. Lianga, F. Yanga, Designing anticancer copper(II) complexes by optimizing 2-pyridine-thiosemicarbazone ligands, Eur. J. Med. Chem. 158 (2018) 442–452.

[16] M. Serda, D.S. Kalinowski, N. Rasko, E. Potuckova, A. Mrozek-Wilczkiewicz, R. Musiol, J.G. Małecki, M. Sajewicz, A. Ratuszna, A. Muchowicz, J. Gołab, T. S. imunek, D.R. Richardson, J. Polanski, Exploring the Anti-Cancer Activity of Novel Thiosemicarbazones Generated through the Combination of Retro-Fragments: Dissection of Critical Structure-Activity Relationships, PLoS One 10 (2014) 1–15.

[17] K. Malarz, A. Mrozek-Wilczkiewicz, M. Serda, M. Rejmund, J. Polanski, R. Musiol, The role of oxidative stress in activity of anticancer thiosemicarbazones, Oncotarget. 25 (2018) 17689–17710.

[18] M. Rejmund, A. Mrozek-Wilczkiewicz, K. Malarz, M. Pyrkosz-Bulska, K. Gajcy, M. Sajewicz, R. Musiol, J. Polanski, Piperazinyl fragment improves anticancer activity of Triapine, PLoS One 13 (2018) 1–25.

[19] M.D. Tomczyk, K.Z. Walczak, l,8-Naphthalimide based DNA intercalators and anticancer agents. A systematic review from 2007 to 2017, Eur. J. Med. Chem. 159 (2018) 393–422.

[20] Z. Tian, Z. Zhao, F. Zang, Y. Wang, Ch. Wang, Spectroscopic study on the interaction between naphthalimide – polyamine conjugates and DNA, J. Photochem. Photobiol. B, Biol. 138 (2014) 202–210.

[21] D. He, L. Wang, L. Wang, X. Li, Y. Xu, Spectroscopic studies on the interactions between novelbisnaphthalimide derivatives and calf thymus DNA, J. Photochem. Photobiol. B, Biol. 166 (2017) 333–340.

[22] L. Ingrassia, F. Lefranc, R. Kiss, T. Mijatovic, Naphthalimides and Azonafides as promising anti-cancer agents, Curr. Med. Chem. 16 (2009) 1192–1213.

[23] Z. Tian, Yingying Huang, Y. Zhang, L. Song, Y. Qiao, X. Xu, Ch. Wang, Spectroscopic and molecular modeling methods to study the interaction between naphthalimide-polyamine conjugates and DNA, J. Photochem. Photobiol. B, Biol. 158 (2016) 1–15.

[24] M.F. Brana, A.M. Sanz, J.M. Castellano, C.M. Roldan, C. Roldan, Synthesis and cytostatic activity of benz(de)isoquinoline-1,3-diones structure activity relationships, Isocyclic Compounds. 16 (1981) 207–212.

[25] R. Al-Salahi, M. Marzouk, Synthesis of novel 2-Amino-benzo[de]isoquinolin-1,3-dione derivatives, Asian J. Chem. 26 (2014) 2166–2172.

[26] R. Al-Salahi, I. Alswaidan, H.A. Ghabbour, E. Ezzeldin, M. Elaasser, M. Marzouk, Docking and antiherpetic activity of 2-Aminobenzo[de]-isoquinoline-1,3-diones, Molecules 20 (2015) 5099–5111.

[27] R. Wodtke, J. Steinberg, M. Kockerling, R. Loser, C. Mamat, NMR-based investigations of acyl-functionalized piperazines concerning their conformational behavior in solution, RSC Adv. 8 (2018) 40921–40933.

[28] H. Zhan, Y. Hu, P. Wang, J. Chen, Molecular structures of gas-phase neutral morpholine and its monohydrated complexes: experimental and theoretical approaches, RSC Adv. 7 (2017) 6179–6186.

[29] N. Sampath, M.N. Ponnuswamy, M. Nethaji, Crystal structure and conformation of a piperidine-containing thiosemicarbazone derivative, Mol. Cryst. Liq. Cryst. (2006) 93–101.

[30] M.N. Ponnuswamy, M.M. Gromiha, S.M.M. Sony, K. Saraboji, Conformational aspects and interaction studies of heterocyclic drugs, Top. Heterocycl. Chem. 3 (2006) 81–147.

[31] B. Testa, G. Vistoli, A. Pedretti, Mechanisms and pharmaceutical consequences of processes of stereoisomerisation — a didactic excursion, Eur. J. Pharm. Sci. 88 (2016) 101–123.

[32] T.D. Phien, L.E. Kuzmina, A. Kvaran, S. Jonsdottir, I. Arnason, S.A. Shlykov, Cyanocyclohexane: axial-to-equatorial "seesaw" parity in gas and condensed phases, J. Mol. Struct. 1168 (2018) 127–134.

[33] M.J. Frisch, G.W. Trucks, H.B. Schlegel, G.E. Scuseria, M.A. Robb, J. Nakatsuji, R. Cheeseman, G. Scalmani, V. Barone, B. Mennucci, G.A. Petersson, H.M. Caricato, X. Li, H.P. Hratchian, A.F. Izmaylov, J. Bloino, G. Zheng, J.L. Sonnenberg, M. Hada, M.Ehar.K. Toyota, R. Fukuda, J. Hasegawa, M. Ishida, T. Nakajima, Y. Honda, O. Kitao, H. Nakai, T. Vreven, J.E.Peralta Montgomery, F. Ogliaro, M.J. Bearpark, J. Heyd, E.N. Brothers, K.N. Kudin, V.N. Staroverov, R. Kobayashi, J. Normand, K. Raghavachari, et al., Gaussian 09 Revision D.01, Gaussian, Inc, 2009.

[34] A.D. Becke, Density-functional thermochemistry. III. The role of exact exchange, J. Chern. Phys. 98 (1993) 5648–5652.

[35] Ch. Lee, W. Yang, R.G. Parr, Development of the Colic-Salvetti correlation-energy formula into a functional of the electron density, Phys. Rev. B 37 (1988) 785–789.

[36] C.M.H. Ferreira, I.S.S. Pinto, E.V. Soares, H.M.V.M. Soares, (Un)suitability of the use of pH buffers in biological, biochemical and environmental studies and their interaction with metal ions – a review, RSC Adv. 5 (2015) 30989–31003.

[37] M. Sokołowska, K. Pawlas, W. Bal, Effect of common buffers and heterocyclic ligands on the binding of Cu(II) at the multimetal binding site in human serum albumin, Bioinorg. Chem. Appl. 725153 (2010) 1–7.

[38] W.J. Ferguson, K.I. Braunschweiger, W.R. Braunschweiger, J.R. Smith, J. J. McCormick, C.C. Wasmann, N.P. Jarvis, D.H. Bell, N.E. Good, Hydrogen ion buffers for biological research, Anal. Biochem. 2 (1980) 300–310.

[39] É.A. Enyedy, N.V. Nagy, É. Zsigó, Ch.R. Kowol, V.B. Arion, B.K. Keppler, T. Kiss, Comparative solution equilibrium study of the interactions of copper(II), Iron(II) and zinc(II) with triapine (3-Aminopyridine-2-carbaldehydeThiosemicarbazone) and related ligands, Eur. J. Inorg. Chem. (2010) 1717–1728.

[40] S. Kotowicz, M. Korzec, M. Siwy, S. Golba, J.G. Malecki, H. Janeczek, S. Mackowski, K. Bednarczyk, M. Libera, E. Schab-Balcerzak, Novel 1,8-naphthalimides substituted at 3-C position: synthesis and evaluation of thermal, electrochemical and luminescent properties, Dyes Pigm. 158 (2018) 65–78.

[41] M. Korzec, S. Kotowicz, R. Rzycka-Korzec, E. Schab-Balcerzak, J.G. Małecki, M. Czichy, M. Łapkowski, Novel β-ketoenamines versus azomethines for organic electronics: characterization of optical and electrochemical properties supported by theoretical studies, J. Mater, Sci. 55 (2020) 3812–3832.

[42] M. Korzec, K. Malarz, A. Mrozek-Wilczkiewicz, R. Rzycka-Korzec, E. Schab-Balcerzak, J. Polański, Live cell imaging by 3-imino-(2-phenol)-1,8-naphthalimides: the effect of ex vivo hydrolysis, Spectrochim. Acta A. Mol. Biomol. Spectrosc. 238 (2020), 118442.

[43] A. Castiñeiras, R. Pedrido, Aurophilicity in gold(I) thiosemicarbazone clusters, Dalton Trans. 41 (2012) 1363–1372.

[44] S. Lee, H. Lee, O.S. Jung, A sandwich-shaped M3L2 zinc(II) complex containing 1,3,5-tris(dimethyl(pyridin-3-yl)silyl)benzene: selective photoluminescence recognition of diiodomethane, Dalton Trans. 46 (2017) 5843–5847.

[45] Ch.G. Claessens, M.J. Vicente-Aranab, Tomás Torres, Post-assembly error-checking in subphthalocyanine based M3L2 metallosupramolecular capsules, Chem. Commun. (Camb.) 47 (2008) 6378–6380.

[46] R. Kant, S. Maji, Recent advances in the synthesis of piperazine based ligands and metal complexes and their applications, Dalton Trans. 50 (2021) 785–800.
[47] É.A. Enyedy, M.F. Primik, Ch.R. Kowol, V.B. Arion, T. Kiss, B.K. Keppler, Interaction of Triapine and related thiosemicarbazones with iron(III)/(II) and gallium(III): a comparative solution equilibrium study, Dalton Trans. 40 (2011) 5895–5905.
[48] G. Pelosi, Thiosemicarbazone metal complexes: from structure to activity, Open Crystallogr. J. 3 (2010) 16–28.
[49] S.I. Orysyk, G.G. Repich, V.V. Bon, V.V. Dyakonenko, V.V. Orysyk, Yu. L. Zborovskii, O.V. Shishkin, V.I. Pekhnyo, M.V. Vovk, Novel Fe(III), Ni(I.I.) Co (III), Cu(II) coordination compounds involving2-[(2-hydroxyphenyl)methylene] hydrazine-N-(2-propenyl)-carbothioamide as ligand: synthesis, crystal structures and spectralcharacteristics, Inorg. Chim. Acta Rev. 423 (2014) 496–503.
[50] É.A. Enyedy, N.V. May, Veronika F.S. Pape, P. Heffeter, G. Szakács, B.K. Keppler, Ch.R. Kowol, Complex formation and cytotoxicity of Triapine derivatives: a comparative solution study on the effect of the chalcogen atom and NH-methylation, Dalton Trans. 49 (2020) 16887–16902.
[51] X. Guo, Ch. Li, W. Wang, Y. Hou, B. Zhang, X. Wang, Q. Zhou, Polypyridyl Co complex-based water reduction catalysts: why replace a pyridine group with isoquinoline rather than quinoline? Dalton Trans. 50 (2021) 2042–2049.
[52] A.Ch. Reiersølmoen, A. Fiksdahl, Pyridine- and Quinoline- Based Gold(III) Complexes: Synthesis, Characterization, and Application, Eur. J. Org. Chem. 19 (2020) 2867–2877.
[53] N.A. Caballero, F.J. Melendez, C. Muñoz-Caro, A. Niño, Theoretical prediction of relative and absolute pKa values of aminopyridines, Biophys. Chem. 124 (2006) 155–160.
[54] R.S. Hosmane, J.F. Liebman, Paradoxes and paradigms: why is quinoline less basic than pyridine or isoquinoline? A classical organic chemical perspective, Struct. Chem. 20 (2009) 693–697.
[55] M. Korzec, S. Senkała, R. Rzycka-Korzec, S. Kotowicz, E. Schab-Balcerzak, J. Polański, A highly selective and sensitive sensor with imine and phenyl-ethynyl-phenyl units for the visual and fluorescent detection of copper in water, J. Photochem. Photobiol. A: Chem. 328 (2019) 111893–111902.
[56] M. Hricovíni, M. Mazúr, A. Sîrbu, O. Palamarciuc, V.B. Arion, V. Brezová, Copper (II) thiosemicarbazone complexes and their proligands upon UVA irradiation: an EPR and spectrophotometric steady-state study, Molecules 23 (2018) 721–737.
[57] A.E. Stacy, D. Palanimuthu, P.V. Bernhardt, D.S. Kalinowski, P.J. Jansson, D. R. Richardson, Structure–Activity relationships of Di-2-pyridylketone, 2-Benzoyl-pyridine, and 2-Acetylpyridine thiosemicarbazones for overcoming pgp-mediated drug resistance, J. Med. Chem. 59 (2016) 8601–8620.
[58] R. Gawecki, K. Malarz, M. Rejmund, J. Polanski, A. Mrozek-Wilczkiewicz, Impact of thiosemicarbazones on the accumulation of PpIX and the expression of the associated genes, J. Photochem. Photobiol. B, Biol. 199 (2019) 1115852.
[59] M. Serda, D.S. Kalinowski, A. Mrozek-Wilczkiewicz, R. Musiol, A. Szurko, A. Ratuszna, N. Pantarat, Z. Kovacevic, A.M. Merlot, D.S. Richardson, J. Polanski, Synthesis and characterization of quinoline-based thiosemicarbazones and correlation of cellular iron-binding efficacy to anti-tumor efficacy, Bioorg. Med. Chem. Lett. 22 (2012) 5527–5531.
[60] A. Mrozek-Wilczkiewicz, K. Malarz, M. Rams-Baron, M. Serda, D. Bauer, F. P. Montforts, A. Ratuszna, T. Burley, J. Polanski, R. Musiol, Iron Chelators and Exogenic Photosensitizers. Synergy through Oxidative Stress Gene Expression, J. Cancer 8 (2017) 1979–1987.